Supplementary Information for

A CO_2/H_2 Fuel Cell: Reducing CO_2 while Generating Electricity

Yan Liu,[‡a] Yawei Li,[‡b,c] Yuanzhen Chen,[a] Ting Qu,[a] Chengyong Shu,[a] Xiaodong Yang,[d] Haiyan Zhu,[c] Shengwu Guo,[a] Shengdun Zhao,[e] Tewodros Asefa,*[f,g] and Yongning Liu*[a]

[a] State Key Laboratory for Mechanical Behavior of Materials, Xi'an Jiaotong University, Xi'an 710049, PR China.

[b] Department of Chemical Engineering, The Pennsylvania State University, University Park, Pennsylvania 16802, USA.

[c] Institute of Modern Physics, Northwest University, Shaanxi Key Laboratory for Theoretical Physics Frontiers, Xi'an 710069, PR China.

[d] College of Materials Science and Engineering, Huaqiao University, Xiamen 361021, Fujian Province, PR China.

[e] School of Mechanical Engineering, Xi'an Jiaotong University, Xi'an 710049, PR China.

[f] Department of Chemistry and Chemical Biology, Rutgers, The State University of New Jersey, Piscataway, New Jersey 08854, USA.

[g] Department of Chemical and Biochemical Engineering, Rutgers, The State University of New Jersey, Piscataway, New Jersey 08854, USA

[‡] These authors contributed equally to this work.

* Correspondences to: (Y.L.) ynliu@mail.xjtu.edu.cn; (T.A.) tasefa@chem.rutgers.edu

Chemicals and reagents

Pt/C (HiSPEC 4000, 40% Pt) was obtained from Johnson Matthey (UK). Raw multiwalled carbon nanotubes (CNTs) (OD: 30-50 nm, length: 10-20 μm) were supplied by Chengdu Organic Chemicals Co., Ltd (Chengdu, China). Hydrophobic carbon paper (0.21 mm in thickness) and PBI membrane (80 μm in thickness) were purchased from Shanghai Hesen Electric Co., Ltd. and Shanghai Shengjun Polymer Technologies Co., Ltd., respectively. $RuCl_3.nH_2O$ was obtained from Shaanxi Kaida Chemical Engineering Co., Ltd. Nitric acid (HNO_3, 65%-68%) and $NaHCO_3$ were provided by Sinopharm Chemical Reagent Co., Ltd. CO_2 (99.999%), N_2 (99.999%) and H_2 (99.999%) were bought from Praxair (Shanghai), Xi'an Taida Gas Company and Xi'an Weiguang Gas Co., Ltd., respectively. CH_4, for reference, was purchased from Shanghai Weichuang Standard Gas Analytical Technology Co., Ltd.

Density functional theory (DFT)-based calculations

DFT calculations were performed using the Vienna *ab initio* simulation package (VASP) 5.4.1.[1] The projector-augmented-wave (PAW) pseudopotential [2,3] was used to treat the core electrons, while the Perdew–Burke–Ernzerhof (PBE) exchange-correlation functional [4] of the generalized gradient approximation (GGA) was used to describe the interactions between the electrons. The kinetic cutoff energy for the plane-wave basis was set as 400 eV. The Gaussian smearing method with smearing widths of 0.01 eV was applied.

To construct the surface slabs, first, the lattice constants of the corresponding bulk phases of RuO_2 were optimized. The bulk phases were optimized until the magnitude of the residual forces on the atoms was less than 0.001 eV/Å. Because RuO_2 (110) is the most prevalent surface among all surface Miller indexes, here only RuO_2 (110) was considered. In all surface calculations, four-layer slabs with the bottom two layers fixed to their bulk position with the top two layers and adsorbates being allowed to fully relax were employed. A 4×1 supercell with a lattice constant of 12.48 Å×6.37 Å was used to treat the CO_2 reduction reaction (CO_2RR). The vacuum spaces between periodic images were at least 10 Å to minimize the interactions between adjacent images. For this supercell, a 2×4×1 Monkhorst–Pack [5] *k*-point mesh gave an energy convergence to less than 0.03 eV/supercell. The electronic convergence criteria were set as 1×10^{-5} eV, and structural optimization was regarded as complete when the magnitude of the forces on the atoms was less than 0.01 eV/Å.

The surface termination was determined using an *ab initio* thermodynamics approach combined with computational hydrogen electrode model.[6,7] In a computational hydrogen electrode model, the chemical potential of proton and electron is expressed as a function of the chemical potential of hydrogen gas and applied potential energy. The content of O is related to the chemical potential of water. Therefore, based on the calculation of single point energies of different surface terminations, hydrogen gas and water, as well as zero-point energy, entropy correction and temperature effects, the surface energies of different surface termination with respect to the applied potential *U* can be

determined based on the differences in the content of surface O and H atoms. The free energy change of proton-coupled electron transfer (PCET) step on adsorbed intermediates was also calculated using computational hydrogen electrode model. The potential (vs. RHE) required to initiate each PCET step was calculated based on the difference between the free energy of the product and that of the reactant. Among all the PCET steps, the one with the largest value was defined as the limiting potential.

Calculation of the rates of production of CH_4 (V_{CH4})

The rate of production of CH_4 by the cell or cell-stack is calculated and using Equation 1 below, based on the concentration of CH_4 produced, the flow rate of CO_2 and the amount of catalyst loaded in the cell or cell-stack:

$$V_{CH4} = \frac{V_{CO2} \times 60 \times C_{CH4} \times \rho_{CH4}}{M_{CH4} \times L_{RuO2}} \quad (1)$$

where V_{CO2} is the flow rate of CO_2 or the gasses at the outlet at the cathode (in mL/min), C_{CH4} is the concentration of CH_4 produced by the reaction and determined by FID (in ppm), ρ_{CH4} is the density of CH_4 (g/L), M_{CH4} is the molar mass of CH_4 (g/mol), and L_{RuO2} is the loading of RuO_2 (g).

In the case of the single cell, the amount of CH_4 is found to be 8 ppm when the flow rate of CO_2 is 308 mL/min and the amount of RuO_2 loaded in the cell stack is 0.1 g. Considering the value of ρ of CH_4 as 0.717 mg/mL under the reaction condition, the rate of production of CH_4 (V_{CH4}) is found to be 66.25 μmol/g_{cat}.h. Working temperature: 170 °C, discharging current 120 mA.

In the case of cell stack, the amount of CH_4 is found to be 105 ppm when the flow rate of CO_2 is 80 mL/min and the amount of RuO_2 loaded in the cell-stack is 0.3 g. Considering the value of ρ of CH_4 as 0.717 mg/mL under the reaction condition, the rate of production of CH_4 (V_{CH4}) is found to be 75.29 μmol/g_{cat}.h. The working temperature is 170 °C and the discharge current is 148 mA.

Calculation of the contribution of current by CO_2RR to the cell's total current (η)

To determine η, the following Equation 2 was applied:

$$\eta = \frac{M_2}{M_1} \quad (2)$$

where M_1 is the total amount of electron transferred in mol during the reaction, and M_2 is the amount of electrons in mol leading to the formation of CH_4. The values of M_1 and M_2 can be determined by using equations 3 and 4, respectively, below:

$$M_1 = \frac{C \times 3600 \times 10^3}{e_c \times NA} \quad (3)$$

$$M_2 = \frac{V_{CO2} \times t \times C_{CH4} \times \rho_{CH4} \times 8}{M_{CH4}} \quad (4)$$

In equation 3, C is the cumulative charge capacity of the cell when the cell is discharging at a certain current for a certain period of time. It can be multiplied by 3600 to obtain the amount of electrons discharged in 1 h. e_c is the charge of each electron (1.602×10^{-19} C) and N_A is Avogadro constant (6.022×10^{23}). The equation is multiplied by 10^3 to express the value of C in mmol, instead of mol. In

equation 4, V_{CO2} is the flow rate of CO_2 or the gases at the outlet at the cathode (in mL/min), t is the discharge time (in min), C_{CH4} is the concentration of CH_4 determined by FID (ppm), ρ_{CH4} is the density of CH_4 (g/L) under the reaction condition, M_{CH4} is the molar mass of CH_4 (in g/mol). As 8 mol of electrons is required to form 1 mol of CH_4 from CO_2, the equation is multiplied by 8.

As an example, when the single cell was let to discharge at 120 mA for 21 min, a cumulative charge capacity of 0.0418 Ah was measured. The concentration of CH_4 under this condition is found to be 8 ppm by GC when a CO_2 flow rate is 308 mL/min. Based on these, the value of η is calculated, as follows. The cumulative charge capacity of 0.0418 Ah corresponds to 150.48 C electrons (as 1 Ah is 3600 C). By taking the relationship between charge and number of electrons into consideration, the number of electrons involved in mol is then 15.60×10^{-4} mol (M_1). Based on the above condition, the molar quantity of CH_4 is calculated to be 9.76×10^{-4} mmol. As 8 mol electrons leads to one mol CH_4, 78.08×10^{-4} mmol electrons (M_2) would be needed to produce 9.76×10^{-4} mmol CH_4. Finally, η cam be calculated as: $\eta = M_2/M_1 = 1.18$ %.

As another example, η for the cell-stack can be calculated as follows. This cell discharges at 148 mA in 23 min, giving a cumulative capacity of 0.055 Ah. Under this condition and at a CO_2 flow rate of 80 mL/min, the concentration of CH_4 is found to be 105 ppm by GC analysis. By following the same procedure as above, the value of η is found to be 3.36 %.

Supporting Figures

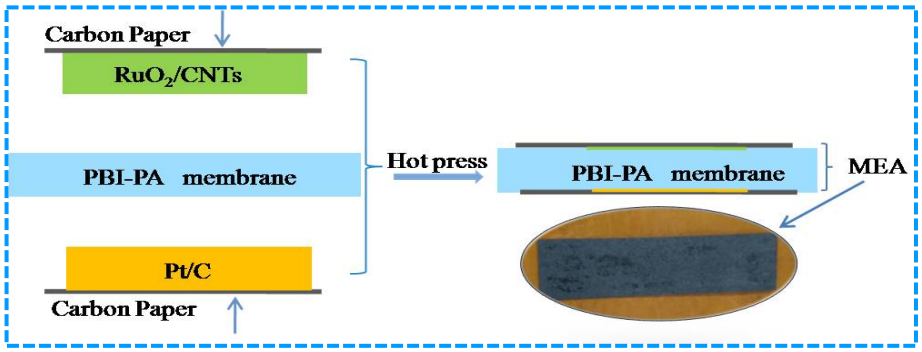

Figure S1. The processes applied to put together the CO_2/H_2 membrane electrode assembly (MEA).

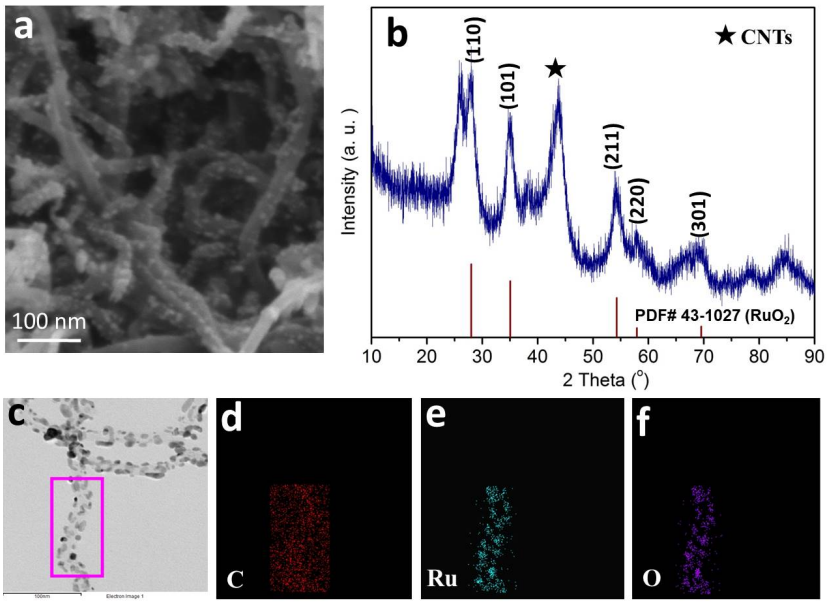

Figure S2. Characterization results for RuO_2/CNTs. (a) SEM image of RuO_2/CNTs. (b) XRD patterns of RuO_2/CNTs. (c) TEM image of RuO_2/CNTs. (d-f) EDS-based elemental mapping images of C, Ru and O in the RuO_2/CNTs, for the sample in the rectangular region of the image shown in (c).

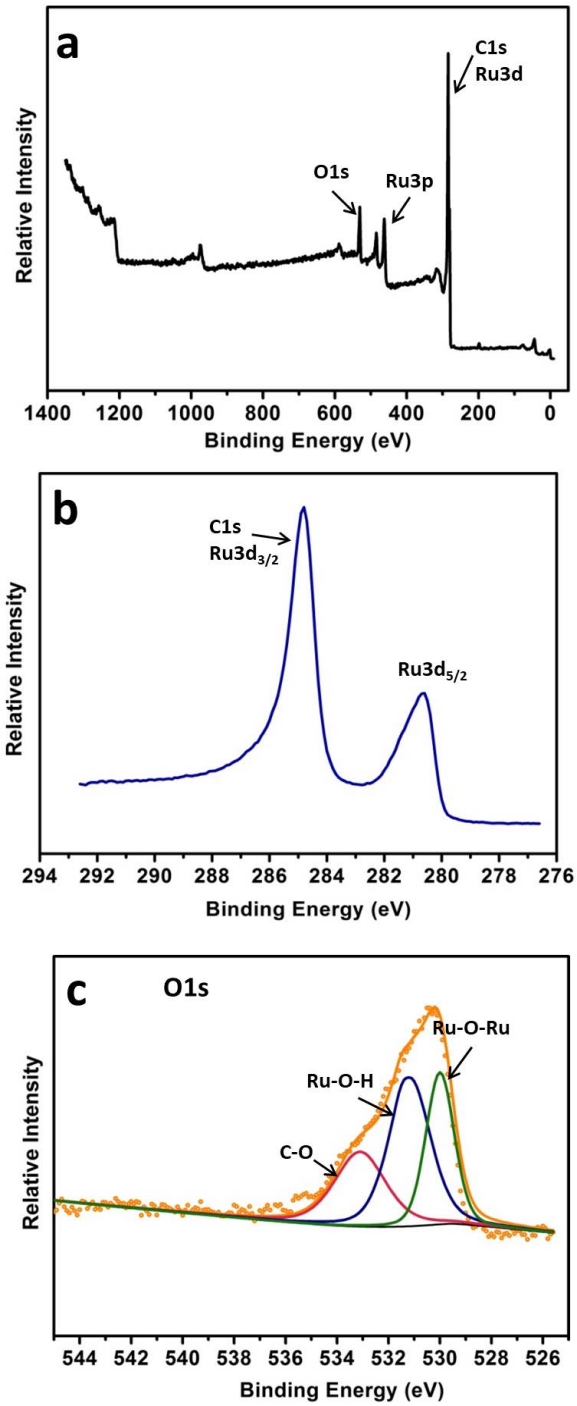

Figure S3. Survey and high-resolution XPS spectra of RuO_2/CNTs. (a) XPS survey spectra of RuO_2/CNTs. (b) High-resolution XPS spectra showing the Ru 3d and C1s peaks of RuO_2/CNTs. (c) High resolution and deconvoluted XPS spectra of O1s peak of RuO_2/CNTs. The spectra of Ru $3d_{3/2}$ and C 1s show overlapping peaks at a binding energy of *ca*. 285 eV, as previously reported.[8,9] The peak at 280.8 eV corresponding to Ru $3d_{5/2}$ is used to identify the electronic states of Ru in the RuO_2/CNTs catalyst and the successful deposition of RuO_2 onto the CNTs. Fig. S3C exhibits the XPS spectrum of O1s with discrete peaks of Ru-O-Ru at 529.5 eV and Ru-O-H at 530.5 eV, and a peak at 531.6 eV corresponding to C-O or surface oxygenated groups.

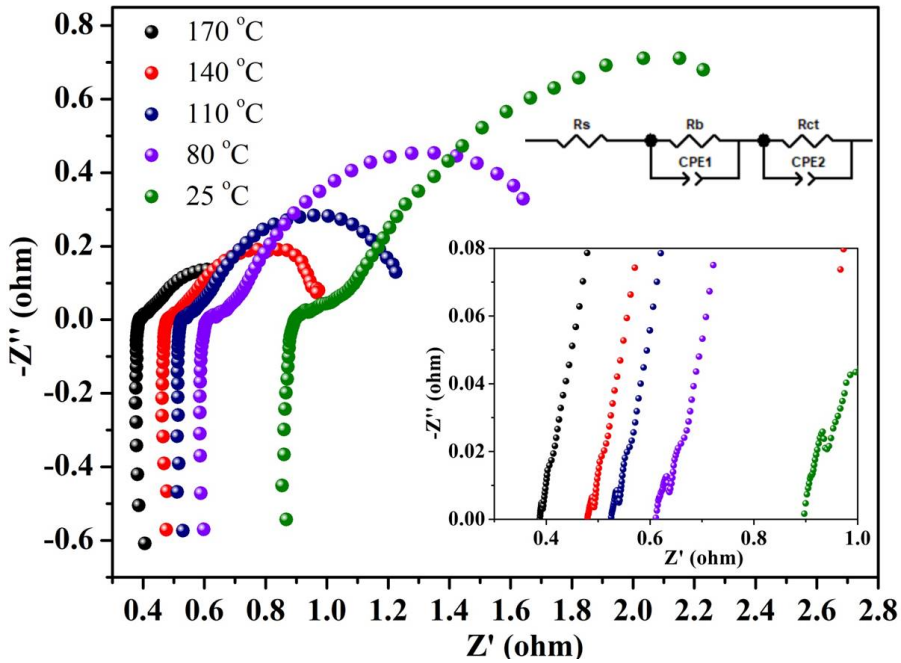

Figure S4. Nyquist plots of the cell working at different temperatures. The insets show the simulated equivalent circuit according to the EIS spectra and the impedance at a high-frequency region.

The high frequency region and simulated equivalent circuit are shown in the insets in there. The observed differences in the Nyquist plots must be due to the different working temperatures, as the cells are the same otherwise. The intersection points on the real axis in a high frequency region are at 0.896 Ω, 0.613 Ω, 0.526 Ω, 0.481 Ω and 0.388 Ω for the operating temperatures at 25 °C, 80 °C, 110 °C, 140 °C and 170 °C, respectively. These values represent the bulk resistance (R_s), which includes the contact resistance, the intrinsic resistance of the active material and the ionic resistance of the electrolyte.[10, 11] The small semicircle at low-frequency region can be ascribed to the charge transfer resistance (R_{ct}).[12] The diameters of the semicircles for the curves obtained at higher temperatures are all small, indicating lower charge transfer resistance (R_{ct}) at these temperatures.[13, 14] The values of calculated R_{ct} for the cells operating at 25 °C, 80 °C, 110 °C, 140 °C and 170 °C are 3.050 Ω, 1.406 Ω, 0.813 Ω, 0.556 Ω and 0.515 Ω, respectively.

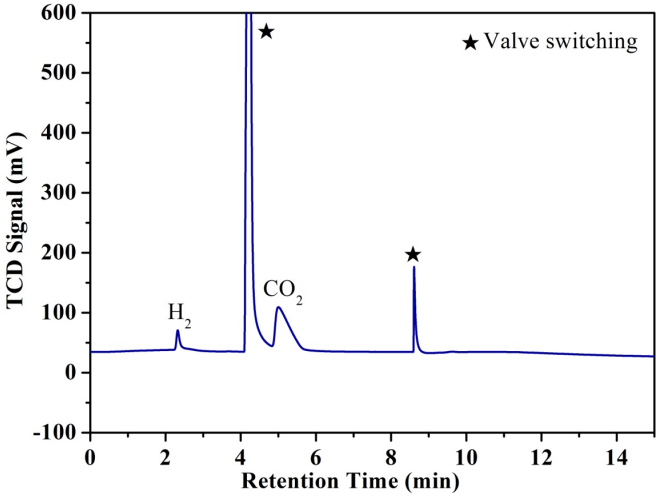

Figure S5. A gas chromatogram obtained with TCD for the product when the cell is operated at 170 °C. The valve switching peaks are caused by the switching of a six-way valve in the GC instrument automatically in order to let different gases enter the detector separately.

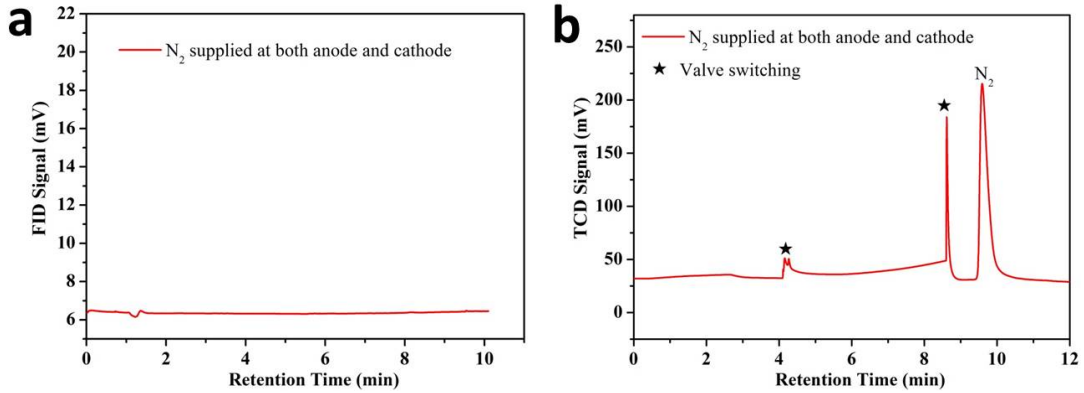

Figure S6. Gas chromatograms obtained when N_2 is supplied at both the anode and cathode compartments of the cell. The measurements are done using (a) FID and (b) TCD. The valve switching peaks are caused by the switching of a six-way valve in the GC instrument automatically in order to let different gases enter the detector separately.

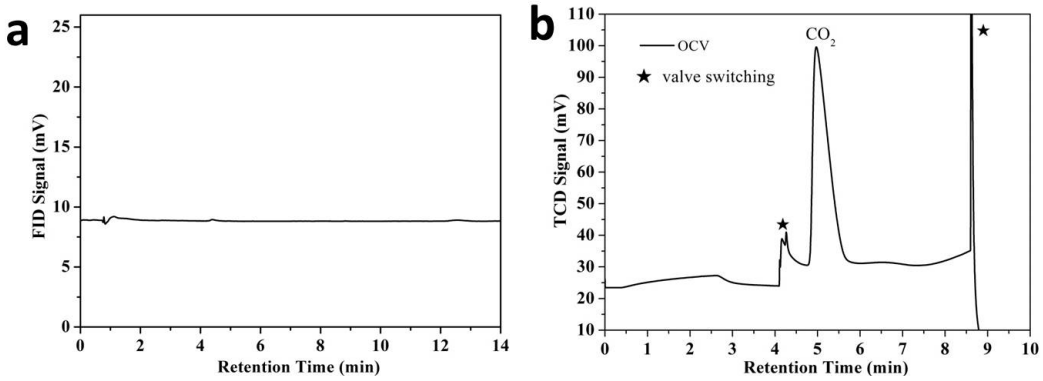

Figure S7. Gas chromatograms obtained when CO_2 is supplied at cathode and H_2 is supplied at anode compartments of the cell under OCV condition. The measurements are done using (a) FID and (b) TCD. The valve switching peaks are caused by the switching of a six-way valve in the GC instrument automatically in order to let different gases enter the detector separately.

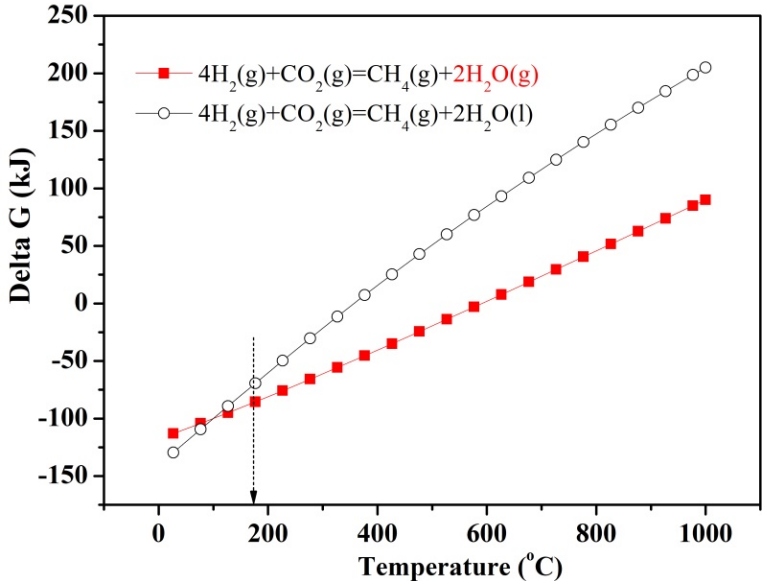

Figure S8. Calculated Gibbs free energy of the reactions at different temperatures.

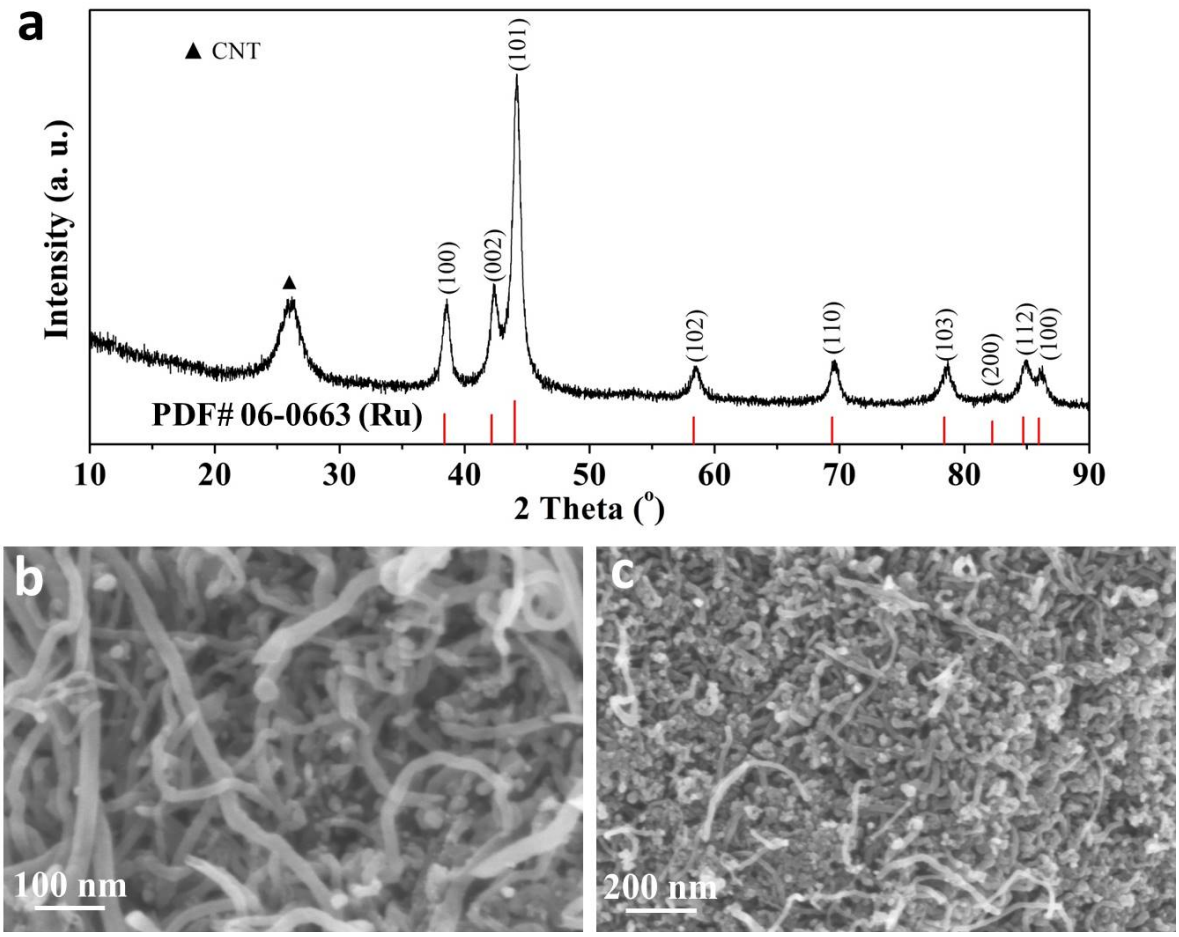

Figure S9. Characterizations of Ru/CNTs. (a) XRD pattern of Ru/CNTs. (b, c) SEM images of Ru/CNTs.

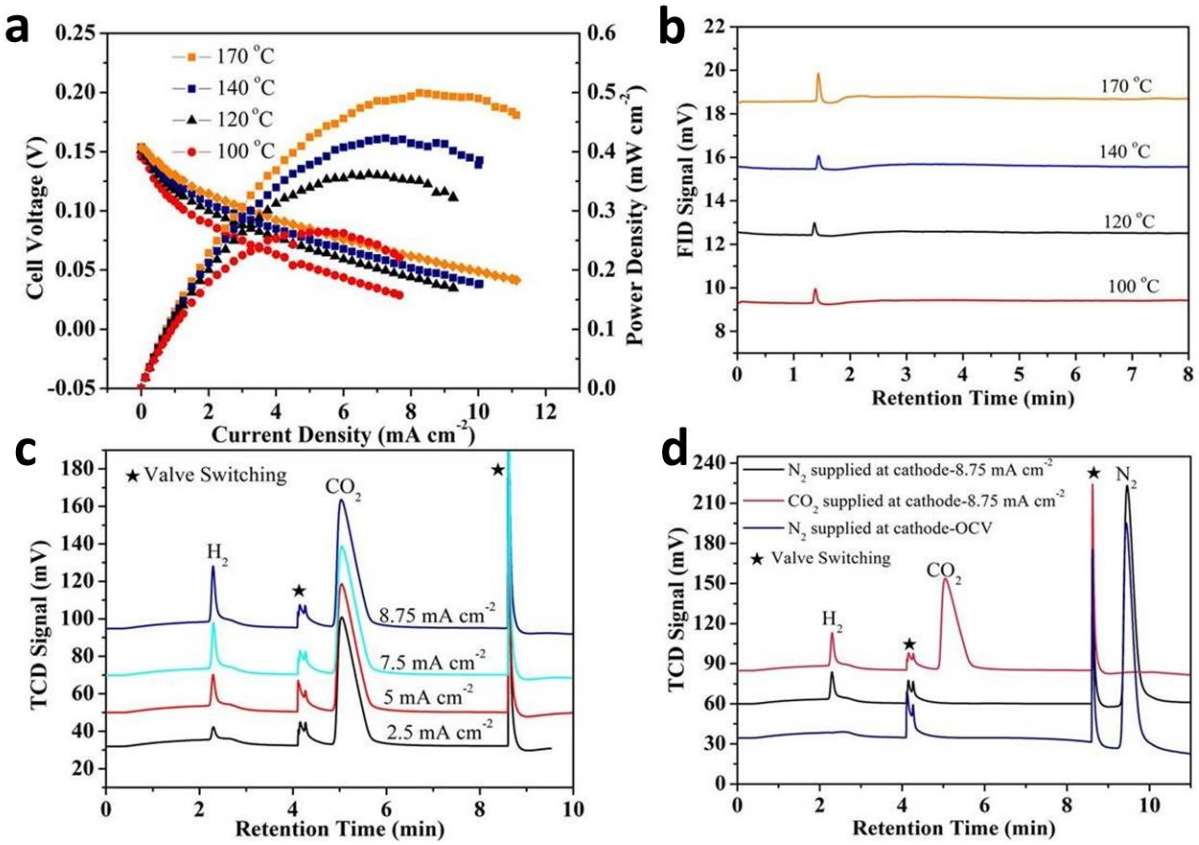

Figure S10. Performances of the cell and analysis of the gaseous products in it when Ru/CNTs are used as cathode catalyst. (a) The performances of the cell at different temperatures. (b) Gas chromatograms obtained using FID when the cell is operating at different temperatures. (c) Gas chromatograms obtained using TCD when the cell is discharging at different current densities at 170 °C. (d) Gas chromatograms obtained with TCD for the gas evolving from the cell when different gases are provided to its cathode and when the cell is operating at 170 °C. The valve switching peaks are caused by the switching of a six-way valve in the GC instrument automatically in order to let different gases enter the detector separately.

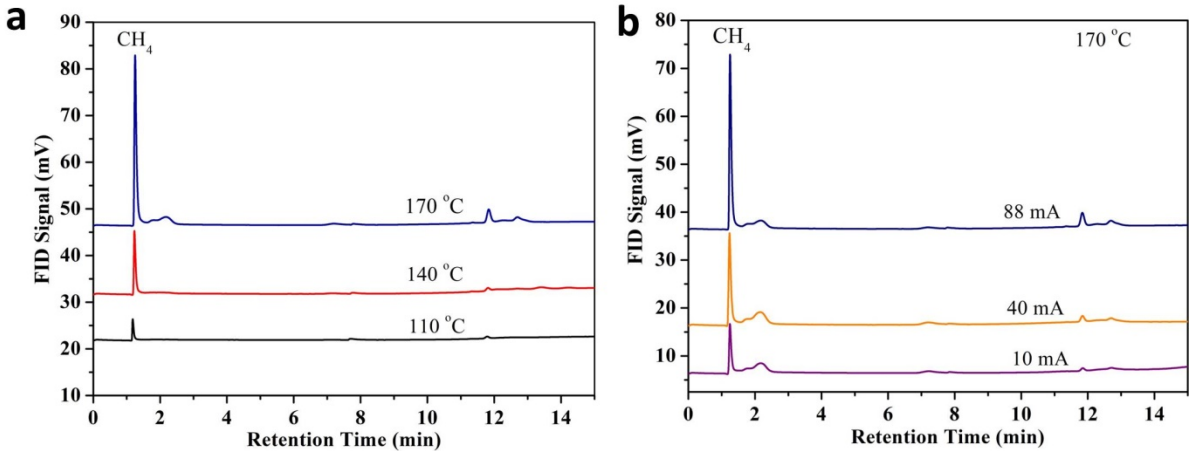

Figure S11. (a) Gas chromatogram obtained with FID detector of the products produced by the cell-stack at different temperatures. (b) Gas chromatogram obtained with FID detector of the products produced by the cell discharging at different current densities at 170 °C.

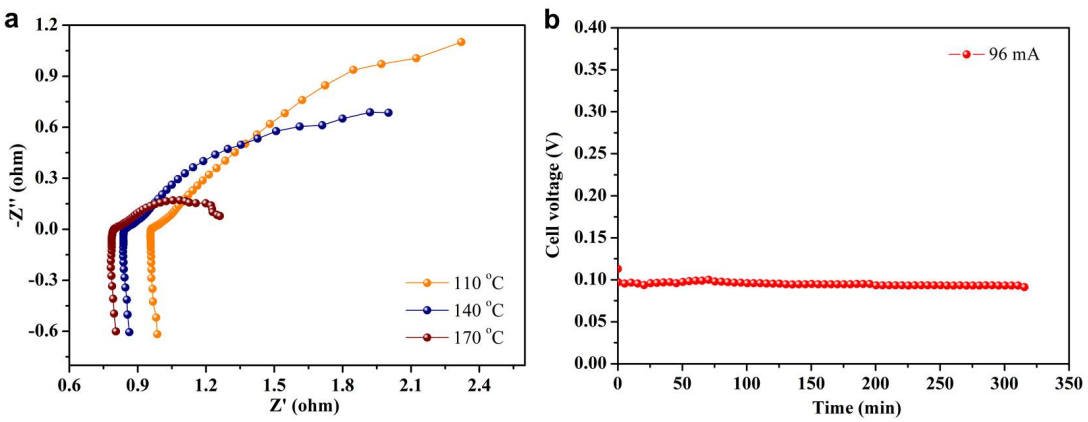

Fig. S12 (a) Nyquist plots of the cell-stack working at different temperatures. (b) Evaluation of the stability of the cell stack at 96 mA and 170 °C.

References

1. G. Kresse and J. Furthmüller, *Phys. Rev. B*, 1996, **54**, 11169-11186.
2. P. E. Blöchl, *Phys. Rev. B*, 1994, **50**, 17953-17979.
3. G. Kresse and D. Joubert, *Phys. Rev. B*, 1999, **59**, 1758-1775.
4. J. P. Perdew, K. Burke and M. Ernzerhof, *Phys. Rev. Lett.*, 1996, **77**, 3865-3868.
5. M. Methfessel and A. T. Paxton, *Phys. Rev. B*, 1989, **40**, 3616-3621.
6. K. Saravanan, Y. Basdogan, J. Dean and J. A. Keith, *J. Mater. Chem. A*, 2017, **5**, 11756-11763.
7. J. K. Nørskov, J. Rossmeisl, A. Logadottir, L. Lindqvist, J. R. Kitchin, T. Bligaard and H. Jónsson, *J. Phys. Chem. B*, 2004, **108**, 17886-17892.
8. Z. J. Han, S. Pineda, A. T. Murdock, D. H. Seo, K. Ostrikov and A. Bendavid, *J. Mater. Chem. A*, 2017, **5**, 17293-17301.
9. X. Fu, H. Yu, F. Peng, H. Wang and Y. Qian, *Appl. Catal. A: Gen.*, 2007, **321**, 190-197.
10. J. Zhang, F. Liu, J. P. Cheng and X. B. Zhang, *ACS Appl. Mat. Interfaces*, 2015, **7**, 17630-17640.
11. F. Cai, Y. Kang, H. Chen, M. Chen and Q. Li, *J. Mater. Chem. A*, 2014, **2**, 11509-11515.
12. S. Chen, G. Yang, Y. Jia and H. Zheng, *J. Mater. Chem. A*, 2017, **5**, 1028-1034.
13. T. Bhowmik, M. K. Kundu and S. Barman, *ACS Appl. Mat. Interfaces*, 2016, **8**, 28678-28688.
14. Z. Chen, H. Xu, Y. Ha, X. Li, M. Liu and R. Wu, *Appl. Catal. B: Environ.*, 2019, **250**, 213-223.